CONFERENCE PRE-PRINT

MATERIAL MIGRATION AND EROSION OF PLASMA-FACING COMPONENTS IN THE FULL-TUNGSTEN WEST TOKAMAK DURING ITS PHASE 1 AND PHASE 2 OPERATIONS

A. HAKOLA, J. LIKONEN
VTT Technical Research Centre of Finland Ltd.
Espoo, Finland
Email: antti.hakola@vtt.fi

M. DIEZ, Y. CORRE, S. DI GENOVA, A. HUART, N. FEDORCZAK, E. TSITRONE
CEA IRFM
Saint-Paul-Lez-Durance, France

J. GASPAR, C. MARTIN
Aix Marseille University
Marseille, France

M. BALDEN, K. KRIEGER
Max-Planck-Institut für Plasmaphysik
Garching, Germany

A. WIDDOWSON
UKAEA, Culham Science Centre
Abingdon, United Kingdom of Great Britain and Northern Ireland

I. BOGDANOVIC RADOVIC, Z. SIKETIC
Ruđer Bošković Institute
Zagreb, Croatia

E. FORTUNA-ZALESNA
Warsaw University of Technology
Warsaw, Poland

E. GRIGORE
National Institute for Laser, Plasma and Radiation Physics
Bucharest, Romania

I. JOGI, P. PARIS
University of Tartu
Tartu, Estonia

M. KELEMEN, S. MARKELJ
Jožef Stefan Institute
Ljubljana, Slovenia

A. LAGOYANNIS, K. MERGIA, P. TSAVALAS
National Centre for Scientific Research “Demokritos”
Athens, Greece

R. MATEUS
IST, University of Lisbon
Lisbon, Portugal

P. PETERSSON
KTH Royal Institute of Technology
Stockholm, Sweden

T. VUORIHEIMO
University of Helsinki
Helsinki, Finland

WEST TEAM*, EUROFUSION TOKAMAK EXPLOITATION TEAM**
*See http://west.cea.fr/WESTteam
** See E. Joffrin et al. 2024 Nucl. Fusion **64** 112019

Abstract

The paper investigates erosion and migration of tungsten (W) in the WEST tokamak during its Phase 1 (2016-2021) and Phase 2 (from 2022) operational phases with a focus on plasma-facing components (PFCs) at the divertor. In Phase 1, gross erosion of PFCs is in line with observations from other major fusion devices and largely caused by low-Z impurities in the plasma. In addition, a strong asymmetry is observed between the high- (inner) and low-field (outer) side divertor targets, in favour of the former. A significant fraction of the eroded W is re-deposited on the PFCs such that net erosion at rates of <0.5 nm/s is measured around the strike points while the remaining areas are dominated by net deposition. The deposited layers in Phase 1 are particularly thick (up to 50 μm) and complex on the high-field side, reflecting the versatile exposure history of the PFCs. The overall erosion-deposition pattern is further influenced by the strong magnetic ripple of WEST, which can result in almost an order of magnitude difference in erosion between the maxima and minima of the ripple in the toroidal direction. In Phase 2, increasing plasma fluence leads to the deposits reaching thicknesses of hundreds of micrometres and a new class of W-containing films, prone to flaking, developing on the surfaces. In the main chamber, erosion is weaker than at the divertor but especially at low densities can result in notable transport of W into the core. Modelling is able to catch many of the observed phenomena in Phase 1, with the exception of the inner-outer asymmetry and the formation of the thick deposits. In contrast, the patterns during the high-fluence operations in Phase 2 require more work.

1. INTRODUCTION

Tungsten (W) is the primary candidate material for the plasma-facing components (PFCs) in future fusion reactors [1]. Tungsten has several advantages over traditionally used low-Z materials such as carbon: W has a high melting point and small erosion yield by impinging plasma particles, in addition to which it shows low activation and retention of plasma fuel during reactor operations. However, as W is a heavy-Z material, even minute W concentrations in the core plasma can lead to considerable radiation losses. In recent years, different plasma-wall interaction (PWI) phenomena as well as the evolution of PFCs upon cumulating exposure to varying plasma discharges has been extensively investigated in several fusion devices with W walls. The tokamaks applied to this end include ASDEX Upgrade (AUG) [2], JET [3], EAST [4], and WEST [5],[6]. In the case of WEST, using superconducting coils offers the possibility of running long plasma discharges and testing several PFC solutions in an ITER-relevant environment.

We investigate here the erosion and deposition behaviour of W during extended plasma exposure in WEST with the focus at the divertor region. In this context, one should distinguish between *gross erosion*, i.e., primary sputtering of W from the wall components, and *net erosion* which takes (prompt) *re-deposition* of W into account [2]. Besides returning on the surface, the sputtered W atoms can migrate in the scrape-off layer (SOL) plasma into new regions and form *co-deposited layers* together with plasma particles and SOL impurities. The structure, composition, and thermo-mechanical properties of the deposits will depend on several parameters including the selected operational conditions and surface characteristics. In future devices, the layers may contain significant amounts of plasma fuel – hydrogen (H), deuterium (D), and tritium (T) – which calls for their detailed investigations during and after a pre-determined series of discharges. The ultimate goal of this work is to obtain insights on the balance between gross and net erosion throughout experimental campaigns on WEST and carry out predictive simulations for future campaigns and devices. The new ITER baseline [7] has even increased the interest in clarifying W erosion and re-deposition patterns everywhere in the reactor vessel.

Data collected from previous experiments on AUG and JET show that large net erosion occurs predominantly close to the outer (low-field side) strike point (OSP), while net deposition typically dominates at the inner strike-point (ISP) region. In the main chamber, net erosion or deposition is an even more local phenomenon, and the determined erosion/deposition rates there can be largely sensitive to changes in the SOL plasma parameters. The results reported hereafter originate from measurements performed during and after several individual experimental campaigns on WEST, and the data will be compared to the established material migration picture in metallic fusion devices, accompanied with results from extensive interpretative modelling efforts.

2. PLASMA OPERATIONS ON WEST AND ANALYSES PERFORMED ON WALL COMPONENTS

WEST is a medium-size tokamak which is capable of producing long plasma pulses (present record 22 minutes [8]) and enable investigating interactions between the PFCs and the plasma in a full-W environment [9]. The operations in WEST have taken place in two distinct phases: Phase 1 from 2016 to 2021 and Phase 2 from 2022 onwards. In Phase 1, the divertor contained a mix of passively-cooled, W-coated graphite plasma-facing units (PFUs) and actively-cooled bulk W tiles, so-called ITER-like PFUs, each consisting of 35 individual monoblocks (MBs). For Phase 2, instead, a full actively-cooled divertor with the above-mentioned MB structure was installed. The limiters in the main chamber consisted of W-coated tiles made of carbon fibre composite while the baffle region as well as the upper divertor were made of actively cooled CuCrZr structures with a W coating [9]. With the exception of the ITER-like PFUs in Phase 1, all the divertor tiles exhibited a 0.5-mm bevel with respect to the neighbouring component to mimic the situation expected in ITER, see Fig. 1 for details.

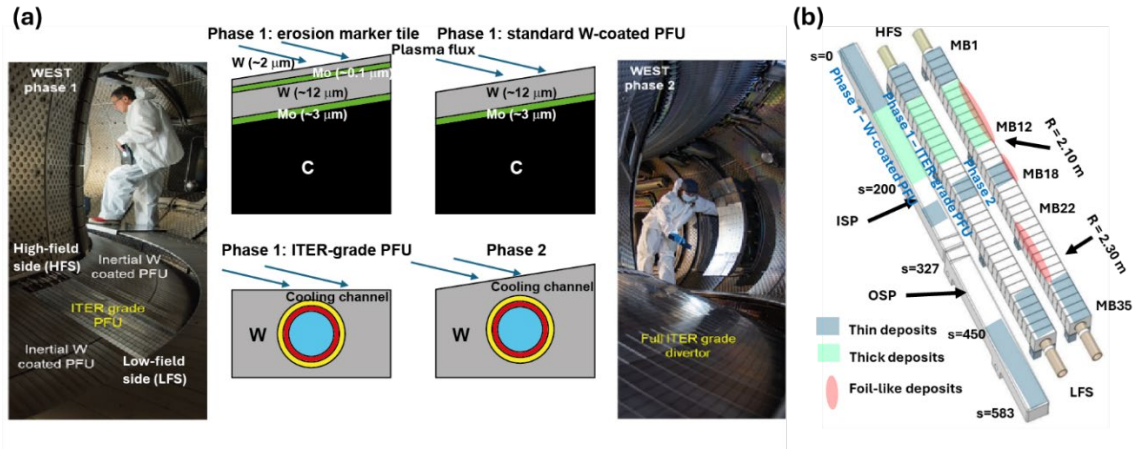

FIG 1. (a) Photographs of the WEST divertor and main-chamber regions (left and right) together with schematic illustrations of the cross-sections of different PFCs in Phase 1 and Phase 2. (b) Schematic layout of WEST PFCs together with the so-called s-coordinate system, naming scheme for the MBs, reference values for the major radius, R, at the divertor as well as characteristic regions on the different PFCs.

Phase 1 consisted of five experimental campaigns (C1-C5, plasma discharges from C2 onwards) whereas up to now 6 campaigns (C6-C11) have taken place in Phase 2, so far without H-mode plasma operations. Glow-discharge boronizations have been regularly performed since the C3 campaign. An overview of the different campaigns is summarized in Table 1. In Phase 2 the main target was on increasing the particle fluence on the divertor target, which was greatly facilitated by the individual discharges being longer than in Phase 1. Worth mentioning are also an extensive helium sub-campaign, performed during C4, and a high-fluence campaign in the end of C7 in attached divertor conditions.

TABLE 1. Key parameters of the WEST experiments in Phase 1 (C2-C5) and Phase 2 (C6-C11)

Campaign/Time	Plasma time	No. boronizations
C2/Nov17-Jan18	~25 min	0
C3/Oct-Dec18	~40 min	3
C4/Sep-Nov19	~3 h 35 min	13
C5/Nov20-Jan21	~1 h 15 min	2
C6+C7/Dec22-Apr23	~5 h 30 min	2
C8+C9/Dec23-Apr24	~5 h 45 min	5
C10+C11/Dec24-Apr25	~7 h	6

Gross erosion of W was primarily assessed via spectroscopic techniques while net erosion was determined via *post mortem* surface analyses for a number of exposed PFCs. During Phase 1, both standard W-coated PFUs and special *erosion marker* PFCs (see Fig. 1) were removed from different toroidal locations of the divertor together with the ITER-like PFUs, separately after the C3, C4, and C5 campaigns. The coated tiles had all a 12-μm thick W coating and a thinner Mo intermediate layer (~3 μm) on graphite, while the marker tiles had additional Mo (~0.1 μm) and W (up to 2 μm) coatings on top to assess campaign-integrated erosion rates. During the

maintenance breaks in Phase 2, several actively cooled MB structures became also available for detailed inspections. Analyses are still ongoing but in the following we will review the first results obtained from them.

For the post-exposure studies, a detailed analysis programme was compiled consisting of both full-tile measurements and more detailed investigations of small samples extracted from the coated PFCs as well as of individual MBs or pieces cut from them. The following methods have contributed to the formation of the database discussed here: (i) visual and microscopy investigations, including scanning electron microscopy (SEM), possibly assisted by focused ion beam (FIB) cuts, and transmission electron microscopy (TEM); (ii) compositional analyses utilizing various ion-beam techniques such as Rutherford backscattering spectrometry (RBS), nuclear reaction analysis (NRA), and time-of-flight elastic recoil detection analysis (TOF-ERDA) as well as energy dispersive X-ray spectroscopy (EDX) during SEM investigations; (iii) elemental depth-profile studies by employing secondary ion mass spectrometry (SIMS), laser-induced breakdown spectroscopy (LIBS), and glow-discharge optical emission spectroscopy (GDOES); (iv) surface-sensitive methods, namely X-ray photoelectron spectroscopy (XPS) and Raman spectroscopy; and (v) thermal desorption spectroscopy (TDS) for obtaining the fuel inventory on the samples. In addition, emissivity measurements were carried out to investigate net erosion of divertor PFCs, both *post mortem* and *in situ* [10].

3. MATERIAL MIGRATION DURING PHASE 1 OPERATIONS ON WEST

3.1. Gross erosion of W in the divertor and main-chamber regions

The determined gross-erosion rates of W during Phase 1 are in line with published data from other tokamaks with full or partial W coverage, peaking to 1-2 nm/s in L-mode plasmas [11],[12]. The strongest W erosion flux is observed at the divertor. Sources at the main chamber are substantially weaker, by one or two orders of magnitude, but upon applying lower hybrid (LH) or ion cyclotron resonance frequency (ICRF) heating notable W emission is observed from the limiter structures surrounding the respective antennas. Sputtering is largely dominated by impurities such as boron (B), carbon (C), nitrogen (N), oxygen (O), and neon (Ne) but equally prominently depends on the SOL plasma conditions, in particular on the electron temperature (T_e). The sputtering rates at the divertor have been measured to 1-2×10^{20} s^{-1} in typical WEST plasmas with the divertor T_e varying from <5 eV to 50 eV at the OSP [11]. Even higher values are possible if the ratio between the ion and electron temperatures upstream is increased, resulting in plasmas becoming hotter at the divertor targets [12].

Another WEST-specific observation is a notable asymmetry in W sputtering between the inner and outer divertor targets: in L-mode sputtering can be a factor of 2-10 higher on the inner side depending on the power entering the SOL as well as plasma density and gas [12], see Fig. 2. Interestingly, the asymmetry shows quite a different dependence from the distribution of fuel or light impurity particles in the divertor SOL. The reason can be associated with the complex interplay between the plasma conditions and impurity profiles responsible for W erosion. Comparison between D and He plasmas shows that gross erosion is more intense in He, by an order of magnitude, and pertains at higher densities than is the case for D plasmas. Moreover, the same inner-outer asymmetry but much more prominently than in the case of D is measured.

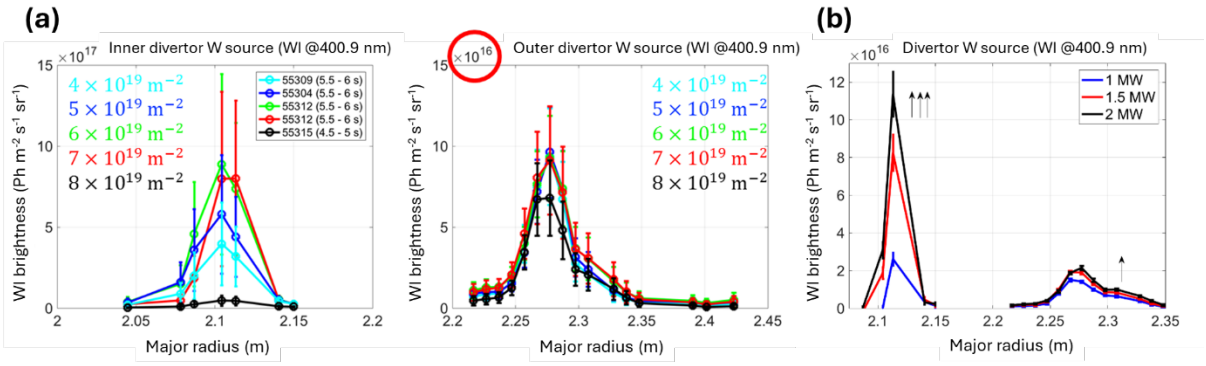

FIG 2. Divertor W sources (based on WI (400.9 nm) line emission) extracted for different L-mode plasmas in (a) helium at different densities and (b) deuterium at varying LH heating powers as a function of the major radius (Fig. 1). The arrows in (b) indicate the trend of increasing brightness with power.

3.2. Net erosion and deposition patterns of W in the divertor

The data obtained from the erosion marker tiles indicate distinct net-erosion regions both at the ISP and OSP regions, as illustrated in Fig. 1b. Somewhat contrary to the data from other metallic devices, also on the inner side the erosion peaks are strong, almost comparable to the values extracted from the vicinity of the OSP. On the other hand, the maximum net-erosion rates are typically in the range of 0.1-0.5 nm/s, in agreement with data from AUG [2]. Locally even higher values are measured because of the strong magnetic ripple of WEST. The ripple introduces toroidal modulation for the particle and power fluxes with a cycle of 18 maxima and minima along the divertor PFCs. To assess the effect of the ripple on erosion, a number of standard W-coated tiles were removed from one sector at the WEST divertor within one ripple period after the C5 campaign and compared to identical, unexposed PFUs. The resulting erosion peaks in the toroidal direction exhibit a factor of 5-10 difference between the high- and low-flux regions and such that the differences are somewhat more prominent on the inner side. The erosion maxima become poloidally shifted by ~20 mm over the ripple cycle and due to the applied beveling and potentially slight misalignment with respect to the nominal position, the peak is toroidally shifted with respect to the central line. More detailed analyses are reported in [13].

In the poloidal direction, the areas dominated by net erosion become more extended from campaign to campaign, with the largest changes occurring between C3 and C4 [5],[6]. In addition, a poloidal shift of the main erosion peaks towards the SOL is observed on both divertor targets from C3 to C5. Generally, the extent of the area dominated by net erosion is ~40-50 mm close to the ISP while it is much wider on the outer side, of the order of 100-120 mm. No proof for the observed asymmetry in gross erosion could be obtained from the *post mortem* analyses since already after the C3 campaign complete erosion of the W markers (>2 μm) was present around the ISP and OSP regions. Concerning helium, it seems not to have introduced notable nanoscale modifications like W fuzz on the surface but is a potential contributor to the above-mentioned poloidal shifts of the erosion maxima.

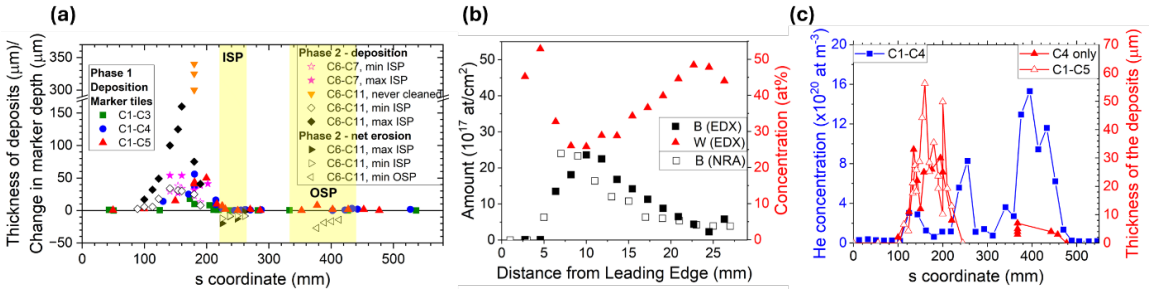

FIG 3. (a) Evolution of the thickness of deposited layers in Phase 1 and Phase 2 together with approximate erosion of marker structures on ITER-like PFUs exposed during Phase 2 as a function of the s coordinate (Fig. 1),(b) B and W content on MB28 (Phase 1) along the toroidal direction, (c) helium content (blue) on standard W-coated PFUs (removed after C4) together with the thickness of deposited layers (red) on similar standard PFUs (data both after C4 and C5).

Notable deposited layers with thicknesses up to 50 μm are measured on the divertor (see Fig. 3a), especially on the inner divertor SOL adjacent to the strike point [5],[6],[14],[15] as well as in a narrow poloidal region where net erosion turns into net deposition on the outer side, see Fig. 1b for details. The thickest layers show complex morphologies with a stratified structure and significant fractions of B, C, and O embedded (Fig. 4a shows an example). In addition, signs of arcing are visible on several locations leading to local damages and delamination of the deposits: up to 25% of the layers or even the underlying coating can be affected. Further into the SOL, both on the inner and outer side, thinner (<0.5 μm) deposited films can be identified almost independent of the exposure campaign. On these layers, the very surface is typically dominated by B and O, followed by distinct sublayers where also metallic impurities such as nickel (Ni), chromium (Cr), iron (Fe), and copper (Cu) are present. In contrast, on the thick deposits no such clear picture can be drawn even though their topmost parts appear to be somewhat enriched in W. The deposits on the ITER-like PFUs are quite similar to the ones discussed above except for the fact that they are 2-5 times thinner [16]. This may be attributed to a smoother surface and the lack of beveling of the MBs but also the different W grade used in the MBs compared to the coated tiles. Concerning fuel retention, the D profiles mainly follow those determined for the low-Z elements proving that the main retention mechanism in Phase 1 is co-deposition. The D concentrations of the deposits are generally <5% and even in the thickest deposits never exceed 20%.

Analogously to the main net-erosion zones discussed above, the areas dominated by deposition become wider or are poloidally shifted as the plasma exposure continues. The thickest deposits during Phase 1 and the most notable changes in their structure and composition are measured after the C4 campaign where the plasma exposure was

considerably longer compared to C3 and several boronizations were carried out. Most of the deposition studies have been performed in a fixed toroidal position, along the central line of the PFCs. More recently additional data has become available also from the toroidal direction. As an example, measurements carried out for an individual MB (MB28) close to the vicinity of the ripple maximum at the OSP region, removed from WEST after the C4 campaign, indicate several characteristic regions in the mm scale. The toroidal leading edge of the MB contains thin deposits with B and N together with metallic impurities and fuel (D and He). The thickness of the deposits increases sharply within a few mm from the leading edge until at ~10 mm – corresponding to one third of the MB extent in the downstream direction – they start to gradually become thinner until only W from the substrate (together with oxygen) remains. This is illustrated in Fig. 3b. Deposition and fuel retention are preferentially concentrated along linear grooves and depressions, showing the local nature of erosion and deposition on technically rough PFCs on WEST [17].

Following the He operations [18] in the end of C4, analyses of the deposits demonstrate noticeable He inventories (corresponding to 5-10 at.%) close to the inner and outer strike points and down to ~140 nm on the surface. This behaviour is depicted in Fig. 3c. The observations suggest that helium would be mainly retained via implantation in the high-flux areas. On the other hand, co-deposition is not completely excluded as shown by a second hump for the He surface density on the peripheral part of the region with thick deposits. On the other hand, deposition deeper inside the deposits cannot be excluded since the TOF-ERDA method used for the analyses is restricted to the vicinity of the PFC surface. Data from various MBs on one actively-cooled PFC give some indications that high He concentrations would occur close to the leading-edge part of the MB but depending on the poloidal position the peak may also be shifted towards the trailing edge [16].

4. IMPACT OF PULSE DURATION AND FLUENCE ON MATERIAL MIGRATION IN PHASE 2

In Phase 2, the experimental activities focused on assessing erosion and migration of W during long pulses and/or at high fluences. At the divertor, the same characteristic regions as after Phase 1 operations emerged: net erosion at the ISP and OSP regions, thick deposits on the SOL side of the inner strike point, and thin films on the remaining areas. Gross erosion rates were comparable to the values measured in Phase 1, indicating that increasing the pulse duration or fluence will not change the established physical picture. The inner-outer asymmetry in W sputtering was again visible, depending on the scenario up to a factor of ~10 larger on the inner than on the outer divertor target [19]. Additional data on the erosion behaviour was obtained from the analyses of so-called fiducial markers [15] on selected MBs after completing individual campaigns in Phase 2. The results demonstrate that net erosion follows the accumulated fluence and is comparable both around the ISP and the OSP. After >18 h of plasma time (from C6 to C11), the depth of the markers around the OSP at the ripple minimum had decreased by ~12-27 μm while at the ISP around the minimum the decrease was ~8 μm; around the ISP ripple maximum the decrease was somewhat larger, 7-20 μm. The patterns can be seen in Fig. 3a. In the main chamber, the strongest sources were again located at the outer midplane, on the limiter structures surrounding the LH antennas, but their gross-erosion rates were at least a factor of two smaller than what was the case at the outer divertor.

The formation of the deposits is concentrated in the inner-divertor region also in Phase 2. Most detailed analyses have been performed after a high-fluence campaign in the end of C7 which consisted of repetitive long L-mode pulses (pulse length 60-70 s) in attached divertor conditions in D (T_e~25 eV) [19]. The accumulated fluence of ~5×10^{26} m^{-2} was reached at the OSP region during some 3 hours of plasma time while the peak surface temperatures remained at modest values of ~400°C. A considerable number of UFOs hampered running the discharges towards the end of the high-fluence campaign phase as deposited layers were piling up [20].

Despite the drastically different operational conditions compared to Phase 1, the deposits were visually similar to the ones observed after preceding campaigns. Fig. 4 shows SEM images of the structure of the thick deposits on an erosion marker tile after C5 (part (a)) and on an ITER-like PFU after the high-fluence campaign (part (b)). The deposited layers continued growing on average and could reach thicknesses of several hundreds of μm (>300 μm) in areas that were not cleaned in between campaigns. All the deposits showed the same complex microstructure as previously reported in [6],[14]: a mixture of low-Z and high-Z elements in a multilayer structure as well as signs of local melting and delamination. The deposits were relatively rich in W in the areas with the highest plasma flux while further into the SOL the light elements O, B, C and N started to dominate the composition. On top of the expected deposits, a new class of foil-like layers was observed, with a tendency to become easily delaminated when exposed to air [15],[21]. These films were only noticed on the magnetically shadowed areas of the MBs, toroidally towards their leading edges. The layers consisted almost exclusively of W and were strongly connected with the high-fluence operations. A photograph of the WEST OSP region after the C9 campaign, showing also the foil-like layers, is included in Fig. 4c.

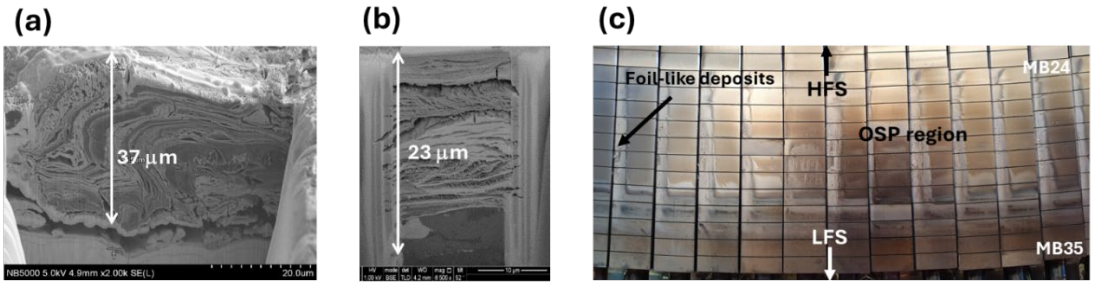

FIG 4. (a,b) SEM cross-sectional images of (a) thick deposits formed in Phase 1 (after C4, s~180 mm, see Fig. 1) and (b) deposits formed during the high-fluence campaign in Phase 2 (after C7, s~150 mm, see Fig. 1); (c) photograph from one sector of the WEST divertor around the OSP region (MB22-MB35, see Fig. 1) after the C9 campaign.

5. MODELLING MATERIAL MIGRATION ON WEST

Tungsten erosion and migration in WEST plasmas has been extensively modelled by SOLEDGE2D/3X and ERO2.0 codes as well as with the help of Particle-In-Cell (PIC) simulations [22], [23] to further elucidate the contributions of the various W sources in the divertor and the main chamber regions. The overall erosion-deposition pattern during Phase 1 can be reproduced by using oxygen as a proxy for the mix of low-Z impurities in the SOL plasma. The most accurate agreement with the experimental data is obtained at low densities (within a factor of 1.5) while in the high-density regime gross erosion is systematically overestimated. The divertor is the strongest W source during typical WEST plasma discharges, however, it is generally well screened over a wide range of background plasma parameters. Instead, the main-chamber region provides a more direct access for the ejected W particles to penetrate into the core. This transport channel is the strongest at low densities due to the sources becoming more efficiently screened at higher densities [24]. Concerning the W content (n_W) of the SOL plasma, the simulations show that n_W is directly proportional to the power entering the SOL (P_{SOL}) as well as to the distance between the separatrix and the LH or ICRH antennas (ROG) [22]. The modelled net-erosion rates, for their part, are sensitive to the applied assumptions for the plasma and transport parameters but also on the material and surface characteristics like the morphology of the PFCs. The main open questions concerning the Phase 1 results are the experimentally observed strong inner-outer asymmetry in gross erosion (section 3.1) and the formation of thick deposits on the inner divertor surfaces (section 3.2). These can be attributed to the role of SOL flows and drifts similarly to what the corresponding studies on AUG have indicated [25]. Further work is also needed to properly account for the 3D structure of erosion patterns on the PFCs.

The modelling efforts in Phase 2 have up to now concentrated on explaining the outcomes of the high-fluence campaign at the divertor [26]. Much emphasis has been put on detailed determination of the fluxes by different impurity ions. The main light impurities in the plasma have been assessed to be B and C while O and N are also present but at smaller concentrations. As a result, the range of impurity levels applied in the simulations could be narrowed down to <5 at.% in terms of the effective O concentration. The simulated gross erosion is almost a factor of 10 higher both at the inner and the outer sides compared to the experimental observations, however, the predicted net erosion appears to be well in line with the experimental data, i.e., a couple of micrometres both at the inner and outer strike-point regions. Instead, the main erosion peaks are predicted poloidally off from the highest flux regions by several centimetres and the thick deposited layers next to the ISP region cannot be reproduced at all. Ongoing work aims at improving the agreement while laboratory investigations are being pursued to provide further insights into the physical mechanisms behind the formation of thick deposits.

6. CONCLUSIONS

We have reported here the extensive investigations aiming at clarifying W erosion and migration in WEST during its Phase 1 and Phase 2 plasma operations. The gross erosion of W is the strongest at the divertor region, however, due to its efficient screening the main-chamber sources may be much more prominent contributors to the transport of W into the core. Minimizing the main-chamber sources shall be achieved by carefully optimizing the applied discharge scenario. The erosion-deposition patterns at the divertor generally agree with literature data from other tokamaks with the exceptions that net erosion is prominent both at the OSP and the ISP and that the deposits can reach values up to hundreds of micrometres if the PFCs are not regularly cleaned. In addition, the strong asymmetry in W sputtering in favour of the inner side is not properly understood but can be the result of a delicate interplay between the plasma flux and impurity atoms in different regions. The increase in pulse duration

and plasma fluence from Phase 1 to Phase 2 does not lead to qualitatively different material migration characteristics in the divertor region except for the deposits becoming even thicker and a new class of foil-like layers starting to form on the tile surfaces. Net erosion of W PFCs during a typical WEST experimental campaign seems not to present insurmountable issues for the lifetime of divertor components when scaling up to future devices while the formation of deposits implies a complicated dependence for their formation on the exposure history of the PFCs.

ACKNOWLEDGEMENTS

This work has been carried out within the framework of the EUROfusion Consortium, funded by the European Union via the Euratom Research and Training Programme (Grant Agreement No 101052200 — EUROfusion). Views and opinions expressed are however those of the author(s) only and do not necessarily reflect those of the European Union or the European Commission. Neither the European Union nor the European Commission can be held responsible for them.

REFERENCES

[1] PHILIPPS, V., J. Nucl. Mater., **415** (2011) S2–S9.
[2] HAKOLA, A. *et al*., Nucl. Fusion **61** (2021) 116006.
[3] BREZINSEK, S. *et al*., Nucl. Fusion **59** (2019) 096035.
[4] DING, R. *et al*., Nucl. Fusion **55** (2015) 023013.
[5] DIEZ, M. *et al*., Nucl. Mater. Energy **34** (2023) 101399.
[6] BALDEN, M. *et al*., Phys. Scr. **96** (2021) 124020.
[7] LOARTE A. *et al*., Plasma Phys. Control. Fusion **67** (2025) 065023.
[8] DUMONT R. *et al.*, "WEST long-pulse achievements in support of next-step fusion devices", this conference
[9] BUCALOSSI, J. *et al*., Nucl. Fusion **62** (2022) 042007.
[10] GASPAR, J. *et al*., Nucl. Fusion **62** (2022) 096023.
[11] VAN ROOIJ, G. J. *et al*., Phys. Scr. **T171** (2020) 014060.
[12] KLEPPER, C. C. *et al*., Plasma Phys. Control. Fusion **64** (2022) 104008.
[13] BALDEN, M. *et al*., "Erosion and redeposition patterns on divertor tiles after exposure in the first operation phase of WEST", 20th International Conference on Plasma-Facing Materials and Components for Fusion Applications (Proc. Int. Conf., Ljubljana, Slovenia, 2025).
[14] HAKOLA, A. *et al*., "Evolution of elemental depth profiles on co-deposited layers at the divertor region of the WEST tokamak during its Phase 1 operations", 20th International Conference on Plasma-Facing Materials and Components for Fusion Applications (Proc. Int. Conf., Ljubljana, Slovenia, 2025).
[15] DIEZ, M. *et al*., "Overview of the results achieved from the characterization program of the WEST plasma facing components (2018-2024)", 20th International Conference on Plasma-Facing Materials and Components for Fusion Applications (Proc. Int. Conf., Ljubljana, Slovenia, 2025).
[16] MARTIN, C. *et al*., Phys. Scr. **96** (2021) 124035.
[17] TSAVALAS, P. *et al*., "Post-mortem analysis of the erosion/deposition pattern on ITER-like actively cooled W-monoblock from the WEST divertor (Phase I)", submitted to Nuclear Fusion.
[18] TSITRONE, E. *et al*., Nucl. Fusion **62** (2022) 076028.
[19] FEDORCZAK, N. *et al*., Nucl. Mater. Energy **41** (2024) 101758.
[20] GASPAR, J. *et al*., Nucl. Mater. Energy **41** (2024) 101745.
[21] MARTIN, C. *et al*., Nucl. Mater. Energy **41** (2024) 101764.
[22] DI GENOVA, S. *et al*., Nucl. Fusion **64** (2024) 126049.
[23] GALLO, A. *et al*., Phys. Scr. **T171** (2020) 014013.
[24] DI GENOVA, S. *et al*., Nucl. Fusion **61** (2021) 106019.
[25] HAKOLA, A. *et al*., Nucl. Mater. Energy **25** (2020) 100863.
[26] HUART, A. *et al*.,"Modeling of erosion/deposition patterns observed during WEST high-fluence campaign", 20th International Conference on Plasma-Facing Materials and Components for Fusion Applications (Proc. Int. Conf., Ljubljana, Slovenia, 2025).